Sorting of Lens Aquaporins and Connexins into Raft and Nonraft Bilayers: Role of Protein Homo-Oligomerization

Jihong Tong, Margaret M. Briggs, David Mlaver, Adriana Vidal, and Thomas J. McIntosh*
Department of Cell Biology, Duke University Medical Center, Durham, North Carolina

ABSTRACT Two classes of channel-forming proteins in the eye lens, the water channel aquaporin-0 (AQP-0) and the connexins Cx46 and Cx50, are preferentially located in different regions of lens plasma membranes (1,2). Because these membranes contain high concentrations of cholesterol and sphingomyelin, as well as phospholipids such as phosphatidylcholine with unsaturated hydrocarbon chains, microdomains (rafts) form in these membranes. Here we test the hypothesis that sorting into lipid microdomains can play a role in the disposition of AQP-0 and the connexins in the plane of the membrane. For both crude membrane fractions and proteoliposomes composed of lens proteins in phosphatidylcholine/sphingomyelin/cholesterol lipid bilayers, detergent extraction experiments showed that the connexins were located primarily in detergent soluble membrane (DSM) fractions, whereas AQP-0 was found in both detergent resistant membrane and DSM fractions. Analysis of purified AQP-0 reconstituted in raft-containing bilayers showed that the microdomain location of AQP-0 depended on protein/lipid ratio. AQP-0 was located almost exclusively in DSMs at a 1:1200 AQP-0/lipid ratio, whereas ~50% of the protein was sequestered into detergent resistant membranes at a 1:100 ratio, where freeze-fracture experiments show that AQP-0 oligomerizes (3). Consistent with these detergent extraction results, confocal microscopy images showed that AQP-0 was sequestered into raft microdomains in the 1:100 protein/lipid membranes. Taken together these results indicate that AQP-0 and connexins can be segregated in the membrane by protein-lipid interactions as modified by AQP-0 homo-oligomerization.

INTRODUCTION

Cell plasma membranes are thought to contain lipid/protein microdomains or ''rafts'' involved in a number of important physiological processes, including signal transduction (4–8), protein trafficking/recycling (9–11), and organization of the cytoskeleton (12,13). These rafts have often been characterized by their insolubility at 4°C in detergents such as Triton X-100 (Sigma-Aldrich, St. Louis, MO) (14–18). Detergent resistant membranes (DRMs) are enriched in cholesterol and sphingolipids such as sphingomyelin (SM) that primarily have saturated hydrocarbon chains, whereas detergent soluble membranes (DSMs) are enriched in membrane phospholipids, such as phosphatidylcholine, with unsaturated hydrocarbon chains (14,16,19–21). In particular, plasma membranes of lens cells, which contain SM, cholesterol, and phosphatidylcholine with unsaturated hydrocarbon chains (22,23), yield DRMs (24,25).

Lens fiber cell membranes contain two classes of channel-forming proteins, aquaporin-0 (AQP-0) and connexins (Cx46 and Cx50). These channels are critical in maintaining the transparency of the lens (26–30) and play roles in the development and architecture of the lens fiber cells (2,31–36). AQP-0 is a passive water channel that allows water to move freely between the cytosol and extracellular fluid (37,38), whereas the connexins form either gap junctions between adjacent cells or hemichannels between cytosol and extracellular space that allow the passive movement of ions and other small molecules (39).

The complex architecture of lens fiber cells and the distributions of AQP-0, Cx46, and Cx50 in the cell membranes have been studied by freeze-fracture and thin-section electron microscopy (1,2,40–46). AQP-0 is found in small clusters and tetragonal aggregates in single membranes, and also in wavy membrane pairs that contain crystalline arrays of AQP-0 in one membrane (40,42,47). AQP-0 aggregates are often concentrated at the lateral surfaces of fiber cells, whereas gap junctions tend to be located at the apical ends of the fiber cells (1), raising the possibility that AQP-0 and the connexins could be sorted into different membrane microdomains. Microdomain sequestration could be involved in regulating the function of these channels, as the activity of the Kir2.1 channel is dependent on whether it is in a raft or nonraft environment (48).

For some cells the membrane distributions of specific aquaporins and connexins have been determined by detergent extraction methods. For example, AQP-5 of parotid duct cells (49), AQP-8 and AQP-9 of hepatocytes (50), Cx32, Cx43, and Cx46 from cultured kidney and Cos-7 cells (51) have all been extracted in DRMs. In the case of lens fiber cells, AQP-0 (52), Cx46 and Cx50 (25) have been extracted in DRMs. However, Cx26 and Cx50 are specifically excluded from DRMs from cultured kidney and Cox-7 cells (51).

Currently there are open questions on the mechanisms by which some transmembrane proteins (TMPs) are brought into rafts microdomains whereas others are excluded from rafts. Possible mechanisms include: 1), direct TMP-lipid interactions (20,53); 2), interactions between the TMP and resident (acylated) raft proteins such as caveolin-1 (54–56); and 3), interactions between the TMP and the cytoskeleton

Submitted May 14, 2009, and accepted for publication August 21, 2009.

*Correspondence: t.mcintosh@cellbio.duke.edu

Editor: Petra Schwille.

0006-3495/09/11/2493/10 $2.00

doi: 10.1016/j.bpj.2009.08.026

(53,57,58). In the lens the cytoskeletal proteins filensin and CP49 interact with AQP-0 (59), and interactions with caveolin-1 seem to be involved in the recruitment to DRMs of AQP-0 (52) and the connexins (25).

In terms of TMP-lipid interactions in sorting between microdomains a factor to consider is protein aggregation or clustering (homo-oligomerization). This is because the line tension (interfacial energy) at the boundary of the TMP and the lipid bilayer gives rise to an energy barrier due to the hydrophobic mismatch that depends on the relative values of the hydrophobic thickness of the TMP and width of the bilayer hydrocarbon region, as well as the elastic properties of the bilayer (60–62). For raft-containing bilayers the hydrocarbon thickness of DRMs can be as much as 25% larger than that of DSMs (21). However, for a given channel-lipid composition, this edge effect depends on the relative lateral dimension of the boundary between protein and lipid, which becomes smaller as the effective diameter of protein complex increases (61,62). It has been suggested (63–66) that protein clustering could play a role in microdomain sorting of proteins. This effect could be relevant for the lens channels because freeze-fracture experiments for AQP-0 in lipid vesicles have shown individual intramembrane particles at a low protein/lipid ratio (1:20,000 mol/mol), some protein clustering at a higher protein/lipid ratio (1:400), and large aggregates or two-dimensional crystalline regions of AQP-0 at an even higher protein/lipid ratio (1:100) (3). In the case of connexins, although aggregates of Cx46 and Cx50 are observed in gap junctions in cells (2,67), there is no evidence for aggregation of connexin hemichannels (67).

In this study, we test the hypothesis that direct TMP-lipid interactions play a role in the sorting of AQP-0, Cx46, and Cx50 between raft and nonraft microdomains. This is done by comparing the detergent solubilities of AQP-0 and the connexins from isolated fiber cell membranes, as well as from reconstituted proteoliposomes with lipid compositions similar to fiber cell membranes, but containing no caveolin or cytoskeletal proteins. We also use confocal microscopy to analyze the distribution of AQP-0, Cx46, and Cx50 in intact giant unilamellar vesicles containing raft microdomains. The role of protein homo-oligomerization in the microdomain distribution of AQP-0 is analyzed by varying the lipid/AQP-0 ratio in the vesicles.

MATERIALS AND METHODS

Materials

Lipids were purchased from Avanti Polar Lipids (Alabaster, AL) and bovine lenses were from Pel-Freez Biological (Bogers, AR). 3,3′-Dilinoleyloxacarbocyanine perchlorate (DiO), Alexa Fluor 555 goat anti-rabbit IgG, and CBQCA Protein Quantification Kit were obtained from Invitrogen (Carlsbad, CA). The detergent *n*-octyl-D-glucopyranoside (OG) was from Anatrace (Maumee, OH). Triton X-100, protease inhibitor cocktail, dimethyl sulfoxide (DMSO), phenylmethylsulphonyl fluoride (PMSF), and cholera toxin B subunit peroxidase conjugate were obtained from Sigma-Aldrich. Rabbit anti-aquaporin-0 affinity purified polyclonal antibody was from Chemicon (Billerica, MA), Immun-Star goat anti-rabbit-HRP conjugate was from Bio-Rad Laboratories (Hercules, CA), and rabbit anti-connexin 50 polyclonal antibody and goat anti-rabbit IgG-HRP conjugate were obtained from Santa Cruz Biotechnology (Santa Cruz, CA). SDS-PAGE reagents, enhanced chemiluminescence HRP solution, Criterion Tris-HCl gel, and nitrocellulose membranes were from Bio-Rad Laboratories.

Isolation of lens fiber cell membranes

For each preparation, 25 bovine lenses were dissected by removing the epithelial tissue and separating the cortex from the nucleus. Cortical fractions were minced into small pieces and homogenized with a Teflon tipped homogenizer in a 2 mM EDTA, 2 mM EGTA, and 10 mM HEPES buffer (pH 8) containing a protease inhibitor cocktail. (Unless otherwise stated, this buffer was used in all experiments.) The material was centrifuged for 20 min at 17,000 $\times$ *g*, followed by two washes. The resulting crude membrane pellet was diluted in buffer and frozen at -100°C until further use.

Membrane protein preparation

AQP-0 was purified following published methods (68,69). The crude membrane fraction was treated with three consecutive washes at 17,000 $\times$ *g* in HEPES buffer containing initially 4 M urea, then 7 M urea, and finally 0 M urea. This material was solubilized in 2% OG in buffer, and the insoluble material was removed by centrifugation at 110,000 $\times$ *g*. The OG-solubilized supernatant was saved as the ''total membrane'' fraction.

The total membrane fraction was loaded on a HiTrap Q FF anion exchange column (Amersham Bioscience, Piscataway, NJ) equilibrated with 1% OG and fractions were eluted with a step gradient of 0 M, 150 mM, 200 mM, and 1 M NaCl in HEPES buffer. Protein concentrations in the fractions were obtained with the CBQCA Protein Quantification Kit.

Reconstitution of proteins into raft-containing lipid bilayers

Raft-containing lipid bilayers were made using techniques described previously (21,70), with a composition of 36:36:25:2:1 dioleoylphosphatidylcholine (DOPC), bovine brain SM, cholesterol, ganglioside GM1, and PEG-ceramide (mol/mol) for all reconstitution experiments. Bilayers formed from these lipids contain DRMs enriched in SM and cholesterol and DSMs enriched in DOPC (21). The lipids were codissolved in chloroform/methanol, which was removed by rotary evaporation. The dried lipids were resuspended at 60°C in 1% OG, 25 mM HEPES, 150 mM NaCl, 1 mM EDTA, and 1 mM dithiothreitol (DTT) at pH 7.4. Proteins solubilized in 1% OG were mixed with the OG-solubilized lipids and dialyzed at room temperature for 4 h followed by 1 day at 4°C against the same buffer, with 0.1 mM PMSF added into the dialysis buffer before the start of dialysis. The dialyzed material was centrifuged at 115,000 $\times$ *g* at 4°C, the pellets were resuspended in 25 mM HEPES buffer (pH 7.4), and the phospholipid and protein compositions of these proteoliposomes were obtained with phosphate assays (71) and PAGE (see below).

Detergent extraction

Separation of DRMs from DSMs used similar procedures to those used on a variety of cells, including lens cells (18,52,72). The crude membrane fractions or reconstituted protein-lipid vesicles were treated for 30 min at 4°C with Triton X-100 at a 1:5 lipid/Triton ratio, before fractionating with a discontinuous sucrose density gradient in 12 mL ultracentrifuge tubes. One milliliter of the detergent-treated sample was mixed in the centrifuge tube with 3 mL of 60% sucrose in HEPES buffer with a matching Triton concentration to achieve a final concentration of 45% sucrose, and then slowly covered with 4 mL layers of 35% and 5% sucrose, also in HEPES buffer with matching Triton concentrations. After centrifugation at 260,000 $\times$ *g* overnight at 4°C, 12 1-mL fractions were taken from top to bottom of the centrifuge tube.

For reconstituted proteoliposomes raft fractions from the density gradients were identified by dot blotting of the raft lipid GM1 with labeled cholera

toxin (63,73). Aliquots from each fraction were dried on a nitrocellulose membrane, blocked with 5% milk in Tris-buffered saline with 0.05% Tween 20 (TBST), and transferred to 5% milk in TBST buffer containing 1:20,000 diluted peroxidase labeled Cholera toxin B subunit. After washing with TBST buffer, the membrane was exposed to enhanced chemiluminescence HRP solution and developed on an x-ray film. For gradient fractions phospholipid content was determined by phosphate assay (71). For most gradients, the cholesterol content of each fraction was calculated assuming similar cholesterol/phospholipid distributions to those previously measured for DRMs and DSMs (74). As a check on these calculated cholesterol values we also directly measured cholesterol content for fractions from some gradients by use of Amplex Red reagent (Invitrogen). Because the Amplex Red assay underestimates the cholesterol content in SM-rich liposomes (75), we added 1% OG to the raft-containing fractions to ensure that all of the cholesterol was accessible to the reagents and added 1% OG and the appropriate sucrose concentrations to standards.

SDS-PAGE and Western blots

The 4–20%, 18-well Criterion Tris-HCl gel was used to run SDS-PAGE for protein samples treated at 1:1 volume ratio with the Laemmli sample buffer containing 10% SDS. Gels were stained using Sypro Ruby protein stain and analyzed using a BioChemi System (UVP BioImaging System, Upland, CA). All gradient experiments were carried out in either duplicate or triplicate with the PAGE from each composition being quite similar. For Western blots, gels were transferred to a nitrocellulose membrane and blocked in 5% w/v milk in TBST buffer. Then 1:2000 rabbit anti-AQP0 in 5% milk in TBST buffer was added, followed by the secondary goat anti-rabbit-HRP conjugate.

LabWorks 4.0 with the UVP BioImaging System was used for protein quantification of the gel fractions. Integrated optical densities were obtained from AQP-0 bands on the gels and the absolute AQP-0 concentrations were calculated by comparison with bands on the same gel of known AQP-0 concentrations in OG obtained from CBQCA assays. This approach was used for lipid/protein fractions because the lipids interfered with the CBQCA assay.

The mole-fraction partition coefficient for AQP-0 from DSM to DRM was calculated from

$$K_p = \left([P]_R/[P]_S\right) \times \left(\left([L]_S + [P]_S\right)/\left([L]_R + [P]_R\right)\right), \quad (1)$$

where $[P]_R$ and $[P]_S$ represent the molar concentrations of AQP-0 in the DRM and DSM phase, respectively, and $[L]_R$ and $[L]_S$ are the molar concentrations of total lipid (phospholipid plus cholesterol) in the DRM and DSM phase, respectively. The apparent free energies of transfer from DSMs to DRMs were obtained using

$$\Delta G_a = -RT \ln\left(K_p\right), \quad (2)$$

where R is the molar gas constant and T is temperature in degrees Kelvin. The thermal energy (RT) is 0.55 kcal/mol at 277°K. We refer to the energies as apparent free energies as an assumption of the calculations was that Triton did not alter the AQP-0 distribution.

Confocal microscopy

Lipid-protein suspensions were prepared as above with the addition of DiO, which selectively labels liquid-disordered (nonraft) bilayers (70,76). Giant unilamellar vesicles (GUVs) were made following the basic procedures of Akashi et al. (77). Drops of the lipid-protein suspensions were dried overnight on a Teflon surface. Then 100 mM of sucrose in distilled water was added and incubated for 3 h at 37°C. The detached lipid cloud was collected, diluted with 100 mM glucose in distilled water, placed on a microscope slide, and covered with a coverslip. Microdomains were observed in GUVs before protein labeling. For visualization of proteins, the rabbit anti-AQP-0, or anti-Cx46, or anti-Cx50 antibody was added to diluted GUVs solution with 1% BSA and incubated at 37°C for 1 h. The solution was washed with 100 mM glucose, the Alexa Fluor 555 goat anti-rabbit IgG at 1:1000 ratio was added and incubated at 37°C, before final washes with 100 mM glucose.

GUVs were observed with a 63× NA 1.4 Plan Apochromat oil objective on a LSM 510 Meta Zeiss Confocal Microscope. Configurations for double channel excitation and the choice of fluorochromes were made to prevent crosstalk and the two colors were scanned using multitrack line switching (78). The DiO lipid label and Alexa Fluor 555 labeled proteins were observed using 488 nm and 543 nm filters, respectively. Quantitative distribution of proteins in GUVs was obtained with the MetaMorph Offline Imaging Software 7.5.6.0 (Molecular Devices, Downingtown, PA).

RESULTS

Protein isolation

Fig. 1 *A* shows a PAGE of the total OG-solubilized cortical material. Previous studies have shown that the bands between 75 kD and 38 kD correspond to Cx50 and Cx46, with the apparent molecular mass of these lens connexins modified by in vivo cleavage and phosphorylation (43,79–81). When applied to an anion exchange column, the band at 27 kD was highly enriched in the fraction eluted at 200 mM NaCl (Fig. 1 *B*) and Westerns blots (Fig. 1 *C*) showed that this band was AQP-0.

Detergent separation experiments

Fig. 2 shows a representative PAGE analysis of the sucrose density gradients from crude membrane fractions, where the

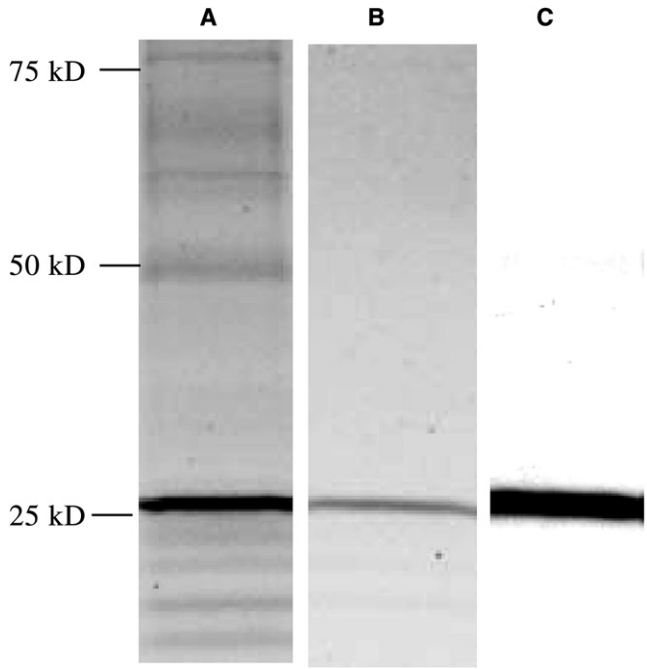

FIGURE 1 Polyacrylamide gels and Western blot of anion exchange column fractions of OG-solubilized lens membrane proteins. Lanes A and B are PAGE of the starting material and column fraction eluted with 200 mM NaCl. Lane C is a Western blot against AQP-0 for that 200 mM column fraction.

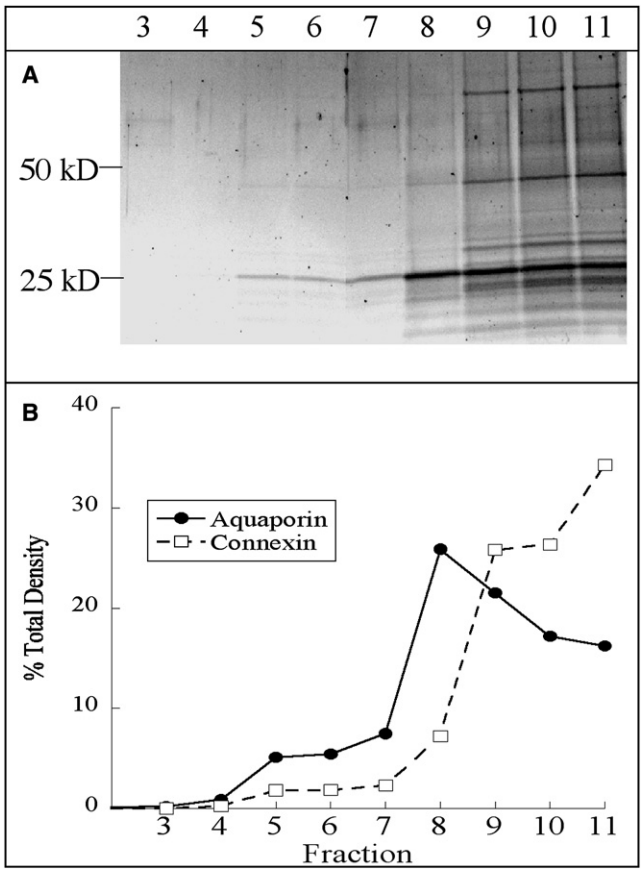

FIGURE 2 (*A*) PAGE of Triton-treated crude lens membranes applied to discontinuous sucrose density gradient. Lighter fractions 3–6 correspond to detergent resistant fractions, whereas heavier fractions 8–11 correspond to detergent soluble fractions. (*B*) Densitometer analysis of the PAGE in *A* with the solid circles showing the AQP-0 band at 27 kD and the *open squares* showing the connexin band at 50 kD.

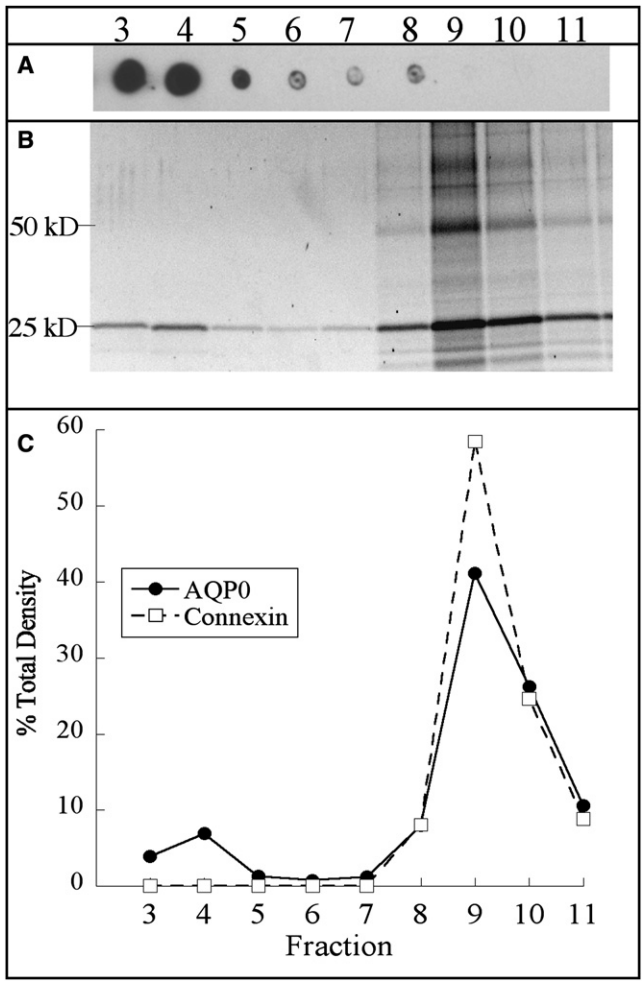

FIGURE 3 OG-solubilized total lens proteins reconstituted in 36:36:25:2:1 DOPC/SM/cholesterol/GM1/PEG-ceramide lipid bilayers were Triton treated and applied to a sucrose density gradient. (*A*) GM1 dot blots of fractions 3–11, indicating that the DRMs were located in the fractions 3–6. (*B*) PAGE of the fractions. (*C*) Densitometer analysis of this PAGE with the solid circles representing the AQP-0 band at 27 kD and the open squares representing the connexin band at 50 kD.

sucrose density increases with increasing fraction number. Previous experiments (18,52) with similar Triton extraction-sucrose density gradients have shown that the lighter fractions correspond to DRMs, whereas the heavier fractions correspond to DSMs. Each protein band in Fig. 2 was more intense in the DSMs. However, as seen in the PAGE (Fig. 2 *A*) and quantified in corresponding densitometer analysis (Fig. 2 *B*), appreciable amounts of the 27 kD (AQP-0) band were also present in the lighter bands 5–7, indicating that DRMs contained more AQP-0 than connexins.

Fig. 3 shows results of Triton extraction experiments of proteoliposomes containing the OG-solubilized total lens proteins in 36:36:25:2:1 DOPC/SM/cholesterol/GM1/PEG-ceramide bilayers. GM1 was enriched in fractions 3–5 (Fig. 3 *A*), indicating that these fractions contained DRMs. On the PAGE (Fig. 3 *B*) the AQP-0 band at 27 kD and the connexin bands at 38 to 70 kD were all more intense in the higher density gradient fractions 8–11, corresponding to DSMs. However, as seen in the PAGE and quantified in Fig. 3 *C*, appreciable amounts of AQP-0 were also located in the DRM fractions 3 and 4. In contrast, no measurable connexin bands were detected in these DRM fractions.

We next considered the possible role of AQP-0 homo-oligomerization on microdomain sorting, taking advantage of the observation detailed in the Introduction that individual AQP-0 tetramers are present in bilayers at low protein/lipid ratios whereas AQP-0 aggregates at higher protein/lipid ratios (3). Fig. 4, *A* and *B*, show GM1 dot blots and PAGE, respectively, of a 1:1200 AQP-0/lipid ratio, whereas Fig. 4, *C* and *D*, show GM1 dot blots and PAGE, respectively, of a 1:100 AQP-0/lipid ratio. Fig. 4 *E* shows results of densitometer traces of the AQP-0 bands from Figs. 4, *B* and *D*, as well as data from an intermediate (1:500 protein/lipid ratio). The amount of AQP-0 in DRM fractions depended on the starting protein/lipid ratio in the proteoliposomes. Specifically, a total of 6% of the AQP-0 was found in

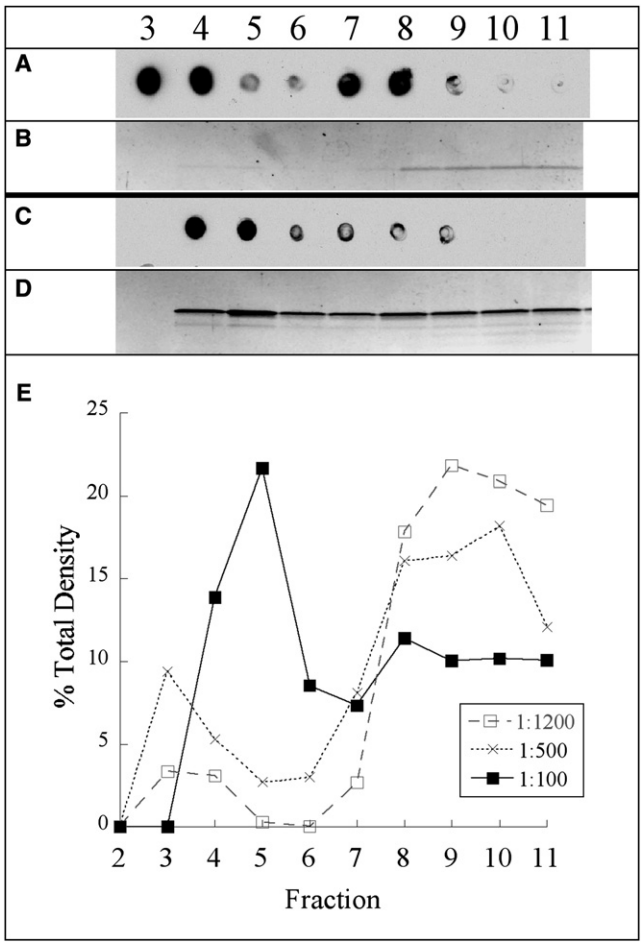

FIGURE 4 Reconstituted proteoliposomes with different AQP-0/lipid molar ratios were treated with Triton and applied to sucrose density gradients. (*A* and *B*) Representative GM1 dot blot and PAGE of the AQP-0 27 kD band, respectively, from the 1:1200 AQP-0/lipid samples. (*C* and *D*) Representative GM1 dot blot and PAGE of the AQP-0 band, respectively, from the 1:100 AQP-0/lipid samples. (*E*) Densitometer analysis of the AQP-0 bands from panels (*B* and *D*) In addition to data from an AQP-0/lipid molar ratio of 1:500, indicating that at low protein/lipid ratio (1:1200) most of the AQP-0 was in the high-density DSM fractions, whereas with increasing protein/lipid ratios more AQP-0 was located in the lighter DRM fractions.

fractions 3–5 for the 1:1200 ratio, whereas 17% of the total AQP-0 was in DRM fractions 3–5 for the 1:500 ratio, and 45% of the total AQP-0 was in DRM fractions 4–6 for the 1:100 ratio. A probable reason for the differences in GM1 distribution (Fig. 4, *A* and *C*) between the DRM fractions is that at the 1:100 ratio appreciably more protein was present in these fractions, making them denser. There was a somewhat variable presence of some GM1 in DSM fractions (Fig. 3 *A* and Fig. 4, *A* and *C*). This may reflect the fact that fractions were collected from the top to the bottom of the gradient, so that GM1 not completely collected in the initial (lighter) fractions ended up in the heavier fractions.

Phosphate assays indicated that the phospholipid was distributed relatively evenly between the DRM and DSM peaks shown in Figs. 2–4. For most gradients we calculated the cholesterol content of each fraction based on these phosphate assays and previous cholesterol and phospholipid measurements (21,75). For comparison, we carried out Amplex red assays of cholesterol for two gradients, at 1:100 and 1:500 AQP-0/lipid ratios (see the Supporting Material), which showed higher cholesterol/total lipid ratios in DRMs than in DSMs. These assays gave cholesterol/total lipid ratios of 0.28 ± 0.13 and 0.25 ± 0.11 for DRM fractions, and 0.15 ± 0.02 and 0.18 ± 0.03 for DSM fractions, similar to the values of 0.32 for DRMs and 0.14 for DSMs calculated from our previous measurements (21,75).

As shown in Fig. 5, when normalized to lipid content, the AQP-0 distribution in the gradient fractions strongly depended on the starting protein/lipid ratio in the reconstituted proteoliposomes. For 1:100 AQP-0/lipid the DRM peak was higher than the DSM peak, whereas for 1:1200 AQP-0/lipid the DRM peak was considerably smaller than the DSM peak.

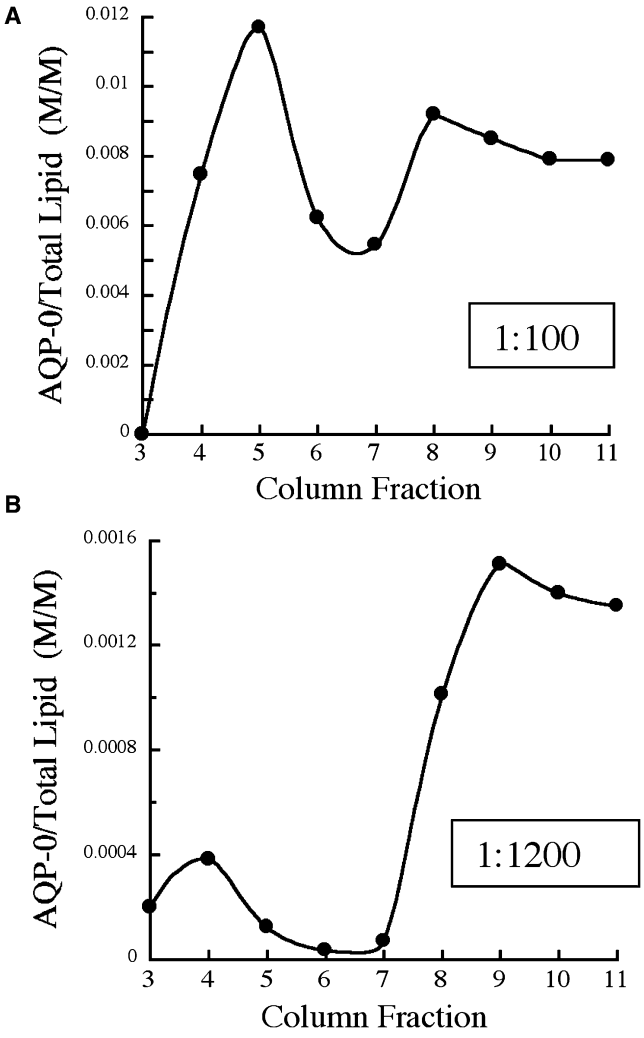

FIGURE 5 Ratios of AQP-0/total lipid in each fraction from sucrose density gradients shown in Fig. 4 for (*A*) 1:100 AQP-0/lipid; and (*B*) 1:1200 AQP-0/lipid.

Equations 1 and 2 were used to calculate the apparent free energy of transfer of AQP-0 from DSMs to DRMs. Using the protein and lipid values of DRM and DSM fractions, we found that $\Delta G_a = -0.1$ kcal/mol for the case of 1:100 AQP-0/lipid. This indicates that it was energetically favorable for AQP-0 to be in DRMs under these conditions, although the magnitude of ΔG_a was smaller than thermal energy (−0.55 kcal/mol). In comparison, $\Delta G_a = +0.7$ and +0.9 kcal/mol for the cases of 1:500 and 1:1200 AQP-0/lipid, respectively. Thus, for these lower protein/lipid ratios it was energetically favorable for AQP-0 to be in DSMs.

Confocal microscopy

Fig. 6 shows confocal images of GUVs formed from proteoliposomes containing total lens protein incorporated into raft-containing bilayers. Each row shows the equatorial plane of a GUV containing the green fluorescent lipid DiO, and the lens proteins labeled with a red fluorescent secondary antibody. Each of the proteins—AQP-0, Cx46, and Cx50—were primarily localized in the nonraft microdomain of the bilayer labeled with DiO. Therefore, all of these channel proteins were enriched in nonraft microdomains, similar to the results obtained with detergent extract experiments from the proteoliposomes of the same compositions (Fig. 3).

Fig. 7 shows confocal images of GUVs formed from proteoliposomes containing different concentrations of purified AQP-0 incorporated into raft-containing bilayers. Equatorial sections through GUVs with a 1:1200 AQP-0/lipid ratio (Fig. 7 *A*) show that at this protein/lipid ratio the AQP-0 was colocalized with the DiO lipid label indicating that the AQP-0 was located primarily in nonraft microdomains. However, in GUVs with a 1:100 AQP-0/lipid ratio (Fig. 7 *B*) some of the AQP-0 was also located in the lipid microdomains that were not labeled with DiO, meaning that at a 1:100 protein/lipid ratio some AQP-0 partitioned into raft microdomains. Quantitative analysis using MetaMorph Offline Imaging software showed that with the 1:1200 protein/lipid ratio almost all of the AQP-0 (99.8% ± 0.7%, mean ± SD, $n = 11$ vesicles) was in nonraft microdomains, whereas at a 1:100 protein/lipid ratio, 61.1% ± 29.4% of the protein was in nonraft domains and 38.9% ± 29.4% was in raft domains ($n = 19$ vesicles). The large standard deviations for the 1:100 protein/lipid experiments were due to heterogeneity in the vesicle population; many observed vesicles, such as those shown in Fig. 7 *B*, contained considerable amount of

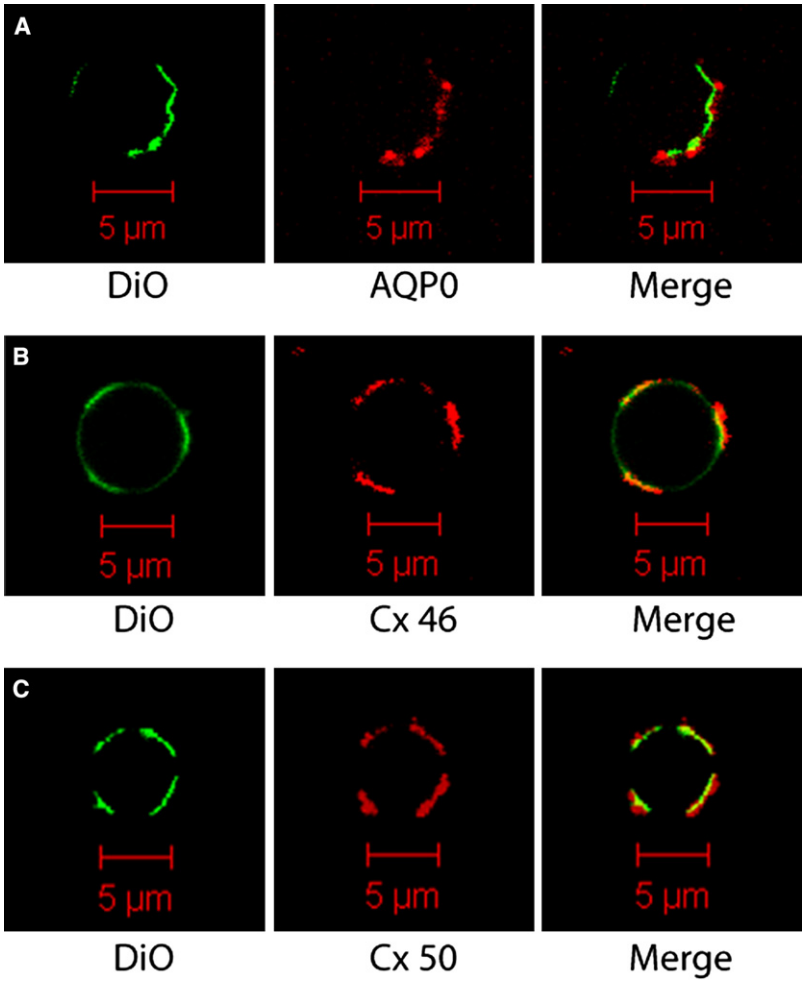

FIGURE 6 Confocal images of equatorial sections of GUVs containing total lens proteins. The *left column* shows the nonraft lipid marker DiO; the middle column shows antibody labeling of AQP-0 (*row A*), Cx46 (*row B*), and Cx50 (*row C*); and the right column is merged images showing both DiO and the antibody-labeled proteins.

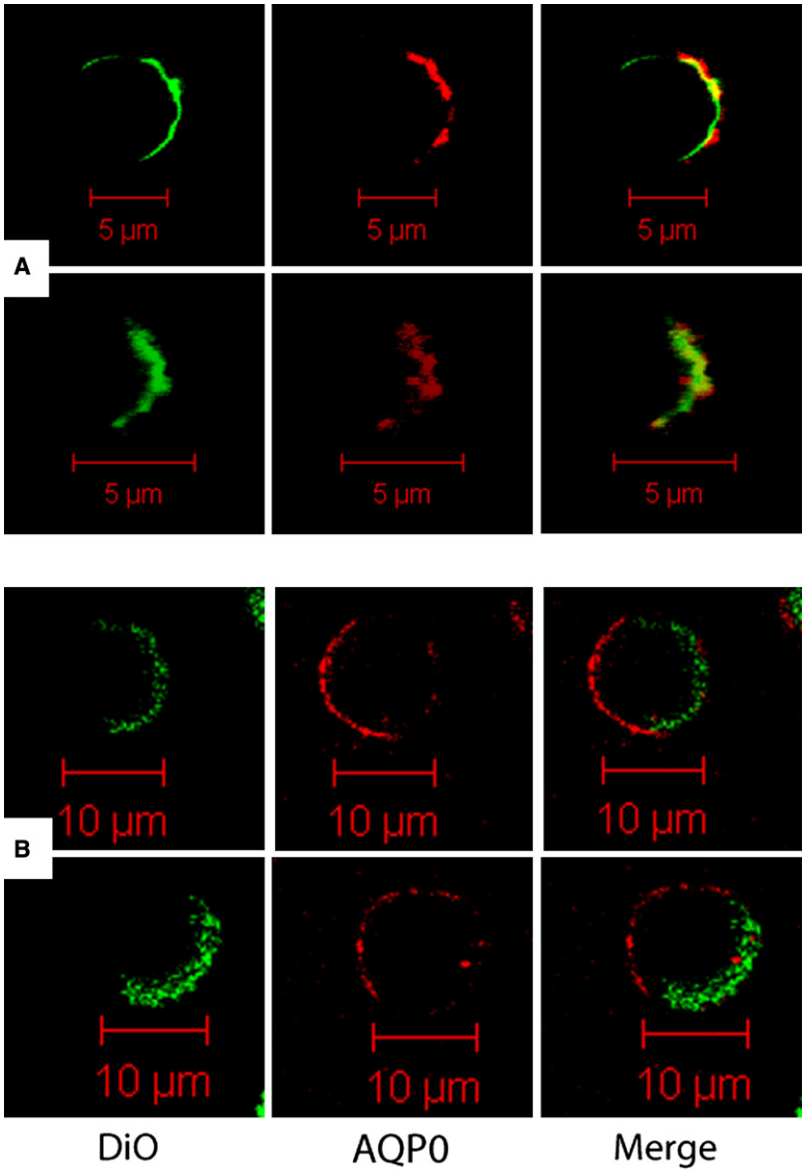

FIGURE 7 Confocal images of equatorial sections of GUVs containing enriched AQP-0 at a 1:1200 protein/lipid ratio (*row A*) and a 1:100 protein/lipid ratio (*row B*). In each row one GUV is shown with the appropriate optical filters so that the left column shows the nonraft lipid label DiO, the center column shows antibody labeled AQP-0, and the right column shows merged images.

protein in the raft portion of the vesicles, whereas a few contained much of the protein in nonraft microdomains.

DISCUSSION

The experiments presented in this study show that AQP-0 and the connexins Cx46 and Cx50 can be sorted in the plane of the lipid bilayer by the formation of lipid microdomains. Triton X-100 extractions of both crude membrane fractions (Fig. 2) and OG-solubilized proteins incorporated into raft containing bilayers (Fig. 3) gave similar results. Both preparations showed that connexins were primarily located in DSMs, whereas AQP-0 was located in DRMs as well as in DSMs. The similarity of the data in Figs. 2 and 3 indicate that our bilayer system of 36:36:25:2:1 DOPC/SM/cholesterol/GM1/PEG-ceramide provided a faithful model for the lipid bilayers in the lens fiber cell membranes.

The detergent extraction experiments with purified AQP-0 incorporated into raft-containing bilayers showed that considerably more AQP-0 was found in DRMs at a high (1:100) AQP-0/lipid ratio, where AQP-0 homo-oligomerizes into crystalline arrays (3), than at a lower (1:1200) AQP-0/lipid ratio (Fig. 5). The AQP-0 distribution from experiments with the entire lens proteins (Fig. 3 *C*), which had peaks in both DRM and DSM fractions, was approximated by the sum of the results from the 1:100 protein/lipid experiments (where there was an appreciable peak in the low-density fractions, Fig. 4, *D* and *E*), and the 1:1200 protein/lipid ratio (where the larger peak was in the high-density fractions, Fig. 4, *B* and *E*). This implies that the proteoliposomes containing the entire lens proteins could contain a mixture of oligomerized and nonoligomerized AQP-0s.

Confocal microscopy images (Fig. 7) were consistent with the detergent extraction results as they showed that in

vesicles AQP-0 was found in both raft and nonraft domains at 1:100 AQP-0/lipid ratio, but highly enriched in nonraft domains at a 1:1200 lipid/protein ratio. Thus, two distinct methods, using very different physical principles, gave similar information on the in-plane bilayer localization of AQP-0 in raft-containing bilayers.

Possible mechanism of protein sorting

Possible mechanisms that could laterally partition unacylated membrane channels into rafts include interactions between the channel and: 1), resident raft proteins such as caveolin (54,55); 2), the cytoskeleton (57,58); and 3), bilayer lipids (20). Depending on the channel, each of these mechanisms could play a role.

Let us first consider interactions of lens channel proteins with caveolin and the cytoskeleton. In terms of the connexins, Lin et al. (25) have shown that there is an association between caveolin-1 and Cx46 and Cx50 that sequesters these connexins to DRMs from whole rat lenses. However, Schubert et al. (51) have shown that Cx50 is excluded from raft microdomains in cultured cells containing caveolin, although other connexins such as Cx32, Cx36, and Cx46 interact with caveolin and are found in raft microdomains. The differences between these two sets of experiments for Cx50 are unclear. Our experiments with crude membrane fractions (Fig. 2) are consistent with the results of Schubert et al. (51) for Cx50, but not for Cx46. Our experiments with lens proteins reconstituted in raft-containing bilayers (Figs. 3–6) show that connexin-lipid interactions alone result in Cx46 and Cx50 being primarily in nonraft microdomains. In terms of AQP-0, it has been shown that AQP-0 interacts with filensin and CP49 (59). Our studies with purified AQP-0 reconstituted into raft-containing bilayers (Figs. 4–7) show that interactions between AQP-0 and bilayer lipids can sequester AQP-0 into raft microdomains even in the absence of caveolin and cytoskeletal proteins.

In terms of channel-lipid interactions in raft sorting, for uncharged lipid bilayers there are three main factors to consider: 1), hydrophobic mismatch (60,61,82) between the hydrophobic length of the channel protein and the width of the hydrocarbon regions of raft and nonraft bilayers; 2), bilayer elastic properties (as modified by cholesterol concentration) (61); and 3), protein clustering (63–66). Due to their high concentration of cholesterol and SM with its long, mostly saturated hydrocarbon chains, raft bilayers are thicker than nonraft bilayers (21). Therefore, just considering hydrophobic mismatch, proteins with long transmembrane domains matching the thickness of SM/cholesterol bilayers would be expected to be in rafts, with shorter proteins in nonrafts. However, bilayer elasticity must be considered in microdomain protein sorting, because the energy of inserting a protein into a bilayer depends on the bilayer elasticity (61), and micropipette experiments (83) indicate that the area compressibility moduli of raft bilayers are ~10 times that of a typical nonraft bilayer. Thus, differences in elasticity between raft and nonraft bilayers would tend to sort transmembrane proteins into nonraft microdomains. These predicted effects of bilayer elasticity have been demonstrated by experiments finding that, regardless of their length, single-pass transmembrane peptides preferentially sort into nonraft bilayers (70,74,84).

The third factor of protein clustering is potentially important because the line tension at the boundary of the channel and bilayer gives rise to an energy barrier that depends on the relative values of protein length, bilayer thickness, and bilayer elasticity. However, for a given channel-lipid composition this edge effect becomes smaller as the effective lateral dimension of the channel increases and it has been proposed that protein clustering could modify microdomain sorting (63–66). In our experiments we varied AQP-0 clustering by changing the protein/lipid ratio in the bilayer, with all other factors remaining constant. Our detergent extraction (Figs. 4–7) and confocal experiments (Figs. 6 and 7) both showed that the sequestration of AQP-0 into raft microdomains was markedly increased under conditions where homo-oligomerization has been observed (3). AQP-0 homo-oligomerization affected the energy balance of raft to nonraft partitioning; ΔG_a changed from $+0.9$ kcal/mol to -0.1 kcal/mol under conditions where AQP-0 oligomerizes. Although a number of assumptions were made in calculating ΔG_a, the relatively large difference between these values (1.0 kcal/mol $= 1.8\,RT$) indicates that homo-oligomerization helped overcome the energy barrier required to sequester AQP-0 into rafts.

Thus, our data suggest that protein-lipid interactions, as modified by AQP-0 homo-oligomerization, can be a key factor in the in plane sorting of channel proteins in lens cell membranes.

SUPPORTING MATERIAL

A figure is available at http://www.biophysj.org/biophysj/supplemental/S0006-3495(09)01388-5.

We thank Ms. Nidhi Tripathi, Mr. Jonathan Faye, and Mr. Kevin Li for excellent laboratory work, Dr. Tim Oliver for help with confocal microscopy, and Drs. Sidney Simon and Michael Bruno for useful discussions.

This work was supported by the National Institutes of Health (GM27278) and by the Howard Hughes Research Fellows Program.

REFERENCES

1. Zampighi, G. A., S. Eskandari, J. E. Hall, L. Zampighi, and M. Kreman. 2002. Micro-domains of AQP0 in lens equatorial fibers. *Exp. Eye Res.* 75:505–519.
2. Dunia, I., C. Cibert, X. Gong, C. H. Xia, M. Recouvreur, et al. 2006. Structural and immunocytochemical alterations in eye lens fiber cells from Cx46 and Cx50 knockout mice. *Eur. J. Cell Biol.* 85:729–752.
3. Ehring, G. R., G. Zampighi, J. Horwitz, D. Bok, and J. E. Hall. 1990. Properties of channels reconstituted from the major intrinsic protein of lens fiber membranes. *J. Gen. Physiol.* 96:631–664.

4. Simons, K., and D. Toomre. 2000. Lipid rafts and signal transduction. *Nat. Rev. Mol. Cell Biol.* 1:31–39.
5. Fielding, C. J., and P. E. Fielding. 2003. Relationship between cholesterol trafficking and signaling in rafts and caveolae. *Biochim. Biophys. Acta.* 1610:219–228.
6. Chini, B., and M. Parenti. 2004. G-protein coupled receptors in lipid rafts and caveolae: how, when and why do they go there? *J. Mol. Endocrinol.* 32:325–338.
7. Young, R. M., X. Zheng, D. Holowka, and B. Baird. 2005. Reconstitution of regulated phosphorylation of FcepsilonRI by a lipid raft-excluded protein-tyrosine phosphatase. *J. Biol. Chem.* 280:1230–1235.
8. He, H. T., A. Lellouch, and D. Marguet. 2005. Lipid rafts and the initiation of T cell receptor signaling. *Semin. Immunol.* 17:23–33.
9. Simons, K., and E. Ikonen. 1997. Functional rafts in cell membranes. *Nature.* 387:569–572.
10. Lafont, F., P. Verkade, T. Galli, C. Wimmer, D. Louvard, et al. 1999. Raft association of SNAP receptors acting in apical trafficking in Madin-Darby canine kidney cells. *Proc. Natl. Acad. Sci. USA.* 96:3734–3738.
11. Ikonen, E. 2001. Roles of lipid rafts in membrane transport. *Curr. Opin. Cell Biol.* 13:470–477.
12. Laux, T., K. Fukami, M. Thelen, T. Golub, D. Frey, et al. 2000. GAP43, MARCKS, and CAP23 modulate PI(4,5)P(2) at plasmalemmal rafts, and regulate cell cortex actin dynamics through a common mechanism. *J. Cell Biol.* 149:1455–1472.
13. Caroni, P. 2001. New EMBO members' review: actin cytoskeleton regulation through modulation of PI(4,5)P(2) rafts. *EMBO J.* 20:4332–4336.
14. Hanada, K., M. Nishijima, Y. Akamatsu, and R. E. Pagano. 1995. Both sphingolipids and cholesterol participate in the detergent insolubility of alkaline-phosphatase, a glycosylphosphatidylinositol-anchored protein, in mammalian membranes. *J. Biol. Chem.* 270:6254–6260.
15. Ahmed, S. N., D. A. Brown, and E. London. 1997. On the origin of sphingolipid/cholesterol-rich detergent-insoluble cell membranes: physiological concentrations of cholesterol and sphingolipid induce formation of a detergent-insoluble, liquid-ordered lipid phase in model membranes. *Biochemistry.* 36:10944–10953.
16. London, E., and D. A. Brown. 2000. Insolubility of lipids in Triton X-100: physical origin and relationship to sphingolipid/cholesterol membrane domains (rafts). *Biochim. Biophys. Acta.* 1508:182–195.
17. Sepulveda, M. R., M. Berrocal-Carrillo, M. Gasset, and A. M. Mata. 2005. The plasma membrane Ca^{2+}-ATPase isoform 4 is localized in lipid rafts of cerebellum synaptic plasma membranes. *J. Biol. Chem.* 281:447–453.
18. Delacour, D., C. I. Cramm-Behrens, H. Drobecq, A. Le Bivic, H. Y. Naim, et al. 2006. Requirement for galectin-3 in apical protein sorting. *Curr. Biol.* 16:408–414.
19. Fridriksson, E. K., P. A. Shipkova, E. D. Sheets, D. Holowka, B. Baird, et al. 1999. Quantitative analysis of phospholipids in functionally important membrane domains from RBL-2H3 mast cells using tandem high-resolution mass spectrometry. *Biochemistry.* 38:8056–8063.
20. Brown, D. A., and E. London. 2000. Structure and function of sphingolipid- and cholesterol-rich membrane rafts. *J. Biol. Chem.* 275:17221–17224.
21. Gandhavadi, M., D. Allende, A. Vidal, S. A. Simon, and T. J. McIntosh. 2002. Structure, composition, and peptide binding properties of detergent soluble bilayers and detergent resistant rafts. *Biophys. J.* 82: 1469–1482.
22. Li, L. K., L. So, and A. Spector. 1985. Membrane cholesterol and phospholipid in consecutive concentric sections of human lenses. *J. Lipid Res.* 26:600–609.
23. Borchman, D., M. C. Yappert, and M. Afzal. 2004. Lens lipids and maximum lifespan. *Exp. Eye Res.* 79:761–768.
24. Rujoi, M., J. Jin, D. Borchman, D. Tang, and M. C. Yappert. 2003. Isolation and lipid characterization of cholesterol-enriched fractions in cortical and nuclear human lens fibers. *Invest. Ophthalmol. Vis. Sci.* 44:1634–1642.
25. Lin, D., S. Lobell, A. Jewell, and D. J. Takemoto. 2004. Differential phosphorylation of connexin46 and connexin50 by H2O2 activation of protein kinase Cgamma. *Mol. Vis.* 10:688–695.
26. Mathias, R. T., J. L. Rae, and G. J. Baldo. 1997. Physiological properties of the normal lens. *Physiol. Rev.* 77:21–50.
27. Mathias, R. T., and J. L. Rae. 2004. The lens: local transport and global transparency. *Exp. Eye Res.* 78:689–698.
28. Stamer, W. D., R. W. Snyder, B. L. Smith, P. Agre, and J. W. Regan. 1994. Localization of aquaporin CHIP in the human eye: implications in the pathogenesis of glaucoma and other disorders of ocular fluid balance. *Invest. Ophthalmol. Vis. Sci.* 35:3867–3872.
29. Gong, X., E. Li, G. Klier, Q. Huang, Y. Wu, et al. 1997. Disruption of alpha3 connexin gene leads to proteolysis and cataractogenesis in mice. *Cell.* 91:833–843.
30. Francis, P., J. J. Chung, M. Yasui, V. Berry, A. Moore, et al. 2000. Functional impairment of lens aquaporin in two families with dominantly inherited cataracts. *Hum. Mol. Genet.* 9:2329–2334.
31. Shiels, A., D. Mackay, S. Bassnett, K. Al-Ghoul, and J. Kuszak. 2000. Disruption of lens fiber cell architecture in mice expressing a chimeric AQP0-LTR protein. *FASEB J.* 14:2207–2212.
32. Shiels, A., S. Bassnett, K. Varadaraj, R. Mathias, K. Al-Ghoul, et al. 2001. Optical dysfunction of the crystalline lens in aquaporin-0-deficient mice. *Physiol. Genomics.* 7:179–186.
33. Verkman, A. S. 2003. Role of aquaporin water channels in eye function. *Exp. Eye Res.* 76:137–143.
34. Al-Ghoul, K. J., T. Kirk, A. J. Kuszak, R. K. Zoltoski, A. Shiels, et al. 2003. Lens structure in MIP-deficient mice. *Anat. Rec. A Discov. Mol. Cell. Evol. Biol.* 273:714–730.
35. White, T. W. 2002. Unique and redundant connexin contributions to lens development. *Science.* 295:319–320.
36. Sellitto, C., L. Li, and T. W. White. 2004. Connexin50 is essential for normal postnatal lens cell proliferation. *Invest. Ophthalmol. Vis. Sci.* 45:3196–3202.
37. Mulders, S. M., G. M. Preston, P. M. Deen, W. B. Guggino, C. H. van Os, et al. 1995. Water channel properties of major intrinsic protein of lens. *J. Biol. Chem.* 270:9010–9016.
38. Varadaraj, K., C. Kushmerick, G. J. Baldo, S. Bassnett, A. Shiels, et al. 1999. The role of MIP in lens fiber cell membrane transport. *J. Membr. Biol.* 170:191–203.
39. Goodenough, D. A., and D. L. Paul. 2003. Beyond the gap: functions of unpaired connexon channels. *Nat. Rev. Mol. Cell Biol.* 4:285–294.
40. Zampighi, G., S. A. Simon, J. D. Robertson, T. J. McIntosh, and M. J. Costello. 1982. On the structural organization of isolated bovine lens fiber junctions. *J. Cell Biol.* 93:175–189.
41. Gruijters, W. T., J. Kistler, S. Bullivant, and D. A. Goodenough. 1987. Immunolocalization of MP70 in lens fiber 16–17-nm intercellular junctions. *J. Cell Biol.* 104:565–572.
42. Costello, M. J., T. J. McIntosh, and J. D. Robertson. 1989. Distribution of gap junctions and square array junctions in the mammalian lens. *Invest. Ophthalmol. Vis. Sci.* 30:975–989.
43. Tenbroek, E., M. Arneson, L. Jarvis, and C. Louis. 1992. The distribution of the fiber cell intrinsic membrane proteins MP20 and connexin46 in the bovine lens. *J. Cell Sci.* 103:245–257.
44. Lo, W. K., A. P. Shaw, L. J. Takemoto, H. E. Grossniklaus, and M. Tigges. 1996. Gap junction structures and distribution patterns of immunoreactive connexins 46 and 50 in lens regrowths of Rhesus monkeys. *Exp. Eye Res.* 62:171–180.
45. Gao, Y., and D. C. Spray. 1998. Structural changes in lenses of mice lacking the gap junction protein connexin43. *Invest. Ophthalmol. Vis. Sci.* 39:1198–1209.
46. Zampighi, G. A., S. Eskandari, and M. Kreman. 2000. Epithelial organization of the mammalian lens. *Exp. Eye Res.* 71:415–435.
47. Costello, M. J., T. J. McIntosh, and J. D. Robertson. 1985. Membrane specializations in mammalian lens fiber cells: distribution of square arrays. *Curr. Eye Res.* 4:1183–1201.

48. Tikku, S., Y. Epshtein, H. Collins, A. J. Travis, G. H. Rothblat, et al. 2007. Relationship between Kir2.1/Kir2.3 activity and their distributions between cholesterol-rich and cholesterol-poor membrane domains. *Am. J. Physiol. Cell Physiol.* 293:C440–C450.

49. Ishikawa, Y., Z. Yuan, N. Inoue, M. T. Skowronski, Y. Nakae, et al. 2005. Identification of AQP5 in lipid rafts and its translocation to apical membranes by activation of M3 mAChRs in interlobular ducts of rat parotid gland. *Am. J. Physiol. Cell Physiol.* 289:C1303–C1311.

50. Mazzone, A., P. Tietz, J. Jefferson, R. Pagano, and N. F. LaRusso. 2006. Isolation and characterization of lipid microdomains from apical and basolateral plasma membranes of rat hepatocytes. *Hepatology.* 43:287–296.

51. Schubert, A. L., W. Schubert, D. C. Spray, and M. P. Lisanti. 2002. Connexin family members target to lipid raft domains and interact with caveolin-1. *Biochemistry.* 41:5754–5764.

52. Cenedella, R. J., P. S. Sexton, L. Brako, W. K. Lo, and R. F. Jacob. 2007. Status of caveolin-1 in various membrane domains of the bovine lens. *Exp. Eye Res.* 85:473–481.

53. Allen, J. A., R. A. Halverson-Tamboli, and M. M. Rasenick. 2007. Lipid raft microdomains and neurotransmitter signaling. *Nat. Rev. Neurosci.* 8:128–140.

54. Lockwich, T. P., X. Liu, B. B. Singh, J. Jadlowiec, S. Weiland, et al. 2000. Assembly of Trp1 in a signaling complex associated with caveolin-scaffolding lipid raft domains. *J. Biol. Chem.* 275:11934–11942.

55. Pike, L. J. 2005. Growth factor receptors, lipid rafts and caveolae: an evolving story. *Biochim. Biophys. Acta.* 1746:260–273.

56. McEwen, D. P., Q. Li, S. Jackson, P. M. Jenkins, and J. R. Martens. 2008. Caveolin regulates kv1.5 trafficking to cholesterol-rich membrane microdomains. *Mol. Pharmacol.* 73:678–685.

57. Oliferenko, S., K. Paiha, T. Harder, V. Gerke, C. Schwarzler, et al. 1999. Analysis of CD44-containing lipid rafts: recruitment of annexin II and stabilization by the actin cytoskeleton. *J. Cell Biol.* 146:843–854.

58. Chichili, G. R., and W. Rodgers. 2007. Clustering of membrane raft proteins by the actin cytoskeleton. *J. Biol. Chem.* 282:36682–36691.

59. Lindsey Rose, K. M., R. G. Gourdie, A. R. Prescott, R. A. Quinlan, R. K. Crouch, et al. 2006. The C terminus of lens aquaporin 0 interacts with the cytoskeletal proteins filensin and CP49. *Invest. Ophthalmol. Vis. Sci.* 47:1562–1570.

60. Mouritsen, O. G., and M. Bloom. 1984. Mattress model of lipid-protein interactions in membranes. *Biophys. J.* 46:141–153.

61. Lundbaek, J. A., O. S. Andersen, T. Werge, and C. Nielsen. 2003. Cholesterol-induced protein sorting: an analysis of energetic feasibility. *Biophys. J.* 84:2080–2089.

62. Andersen, O. S., and R. E. Koeppe. 2007. Bilayer thickness and membrane protein function: an energetic perspective. *Annu. Rev. Biophys. Biomol. Struct.* 36:107–130.

63. Tkachenko, E., and M. Simons. 2002. Clustering induces redistribution of syndecan-4 core protein into raft membrane domains. *J. Biol. Chem.* 277:19946–19951.

64. Draber, P., and L. Draberova. 2002. Lipid rafts in mast cell signaling. *Mol. Immunol.* 38:1247–1252.

65. Bagnat, M., A. Chang, and K. Simons. 2001. Plasma membrane proton ATPase Pma1p requires raft association for surface delivery in yeast. *Mol. Biol. Cell.* 12:4129–4138.

66. Raunser, S., W. Haase, C. Franke, G. P. Eckert, W. E. Muller, et al. 2006. Heterologously expressed GLT-1 associates in ~200-nm protein-lipid islands. *Biophys. J.* 91:3718–3726.

67. Zampighi, G. A. 2003. Distribution of connexin50 channels and hemichannels in lens fibers: a structural approach. *Cell Commun. Adhes.* 10:265–270.

68. Jarvis, L. J., and C. F. Louis. 1995. Purification and oligomeric state of the major lens fiber cell membrane proteins. *Curr. Eye Res.* 14:799–808.

69. Gonen, T., Y. Cheng, J. Kistler, and T. Walz. 2004. Aquaporin-0 membrane junctions form upon proteolytic cleavage. *J. Mol. Biol.* 342:1337–1345.

70. Vidal, A., and T. J. McIntosh. 2005. Transbilayer peptide sorting between raft and nonraft bilayers: comparisons of detergent extraction and confocal microscopy. *Biophys. J.* 89:1102–1108.

71. Chen, Jr., P. S., T. Y. Toribara, and H. Warner. 1956. Microdetermination of phosphorous. *Anal. Chem.* 28:1756–1758.

72. Riddell, D. R., G. Christie, I. Hussain, and C. Dingwall. 2001. Compartmentalization of beta-secretase (Asp2) into low-buoyant density, noncaveolar lipid rafts. *Curr. Biol.* 11:1288–1293.

73. Nguyen, H. T., A. B. Amine, D. Lafitte, A. A. Waheed, C. Nicoletti, et al. 2006. Proteomic characterization of lipid rafts markers from the rat intestinal brush border. *Biochem. Biophys. Res. Commun.* 342:236–244.

74. McIntosh, T. J., A. Vidal, and S. A. Simon. 2003. Sorting of lipids and transmembrane peptides between detergent-soluble bilayers and detergent-resistant rafts. *Biophys. J.* 85:1656–1666.

75. Ayuyan, A. G., and F. S. Cohen. 2008. Raft composition at physiological temperature and pH in the absence of detergents. *Biophys. J.* 94:2654–2666.

76. Kahya, N., D. Scherfeld, K. Bacia, B. Poolman, and P. Schwille. 2003. Probing lipid mobility of raft-exhibiting model membranes by fluorescence correlation spectroscopy. *J. Biol. Chem.* 278:28109–28115.

77. Akashi, K.-I., H. M. Iyata, H. Itoh, and K. Kinosita. 1996. Preparation of giant liposomes in physiological conditions and their characterization under an optical microscope. *Biophys. J.* 71:3242–3250.

78. Tong, J., L. Nguyen, A. Vidal, S. A. Simon, J. H. Skene, et al. 2008. Role of GAP-43 in sequestering phosphatidylinositol 4,5-bisphosphate to Raft bilayers. *Biophys. J.* 94:125–133.

79. White, T. W., R. Bruzzone, D. A. Goodenough, and D. L. Paul. 1992. Mouse Cx50, a functional member of the connexin family of gap junction proteins, is the lens fiber protein MP70. *Mol. Biol. Cell.* 3:711–720.

80. Konig, N., and G. A. Zampighi. 1995. Purification of bovine lens cell-to-cell channels composed of connexin44 and connexin50. *J. Cell Sci.* 108:3091–3098.

81. Kistler, J., J. Berriman, C. W. Evans, W. T. Gruijters, D. Christie, et al. 1990. Molecular portrait of lens gap junction protein MP70. *J. Struct. Biol.* 103:204–211.

82. Killian, J. A. 1998. Hydrophobic mismatch between proteins and lipids in membranes. *Biochim. Biophys. Acta.* 1376:401–416.

83. Rawicz, W., B. A. Smith, T. J. McIntosh, S. A. Simon, and E. Evans. 2008. Elasticity, strength, and water permeability of bilayers that contain raft microdomain-forming lipids. *Biophys. J.* 94:4725–4736.

84. van Duyl, B. Y., D. T. Rijkers, B. de Kruijff, and J. A. Killian. 2002. Influence of hydrophobic mismatch and palmitoylation on the association of transmembrane alpha-helical peptides with detergent-resistant membranes. *FEBS Lett.* 523:79–84.